Article

Distributionally Robust Demand Response for Heterogeneous Buildings with Rooftop Renewables under Cold Climates

Xincong Shi [1,2], Xinrui Wang [3], Yuze Ji [3,*], Zhiliang Liu [1] and Weiheng Han [1]

1   State Grid Shanxi Electric Power Company Limited, Taiyuan 030000, China; yangkm@hlcx.cn (X.S.); lzl20021406@163.com (Z.L.); hwh_scu1986@163.com (W.H.)
2   College of Electrical Engineering, Zhejiang University, Hangzhou 310000, China
3   State Grid Jincheng Power Supply Company, Jincheng 048000, China; wangxr5290@163.com
*   Correspondence: jcjiyuze@163.com

Abstract: A considerable penetration of rooftop PV generation and increasing demand for heating loads will enlarge the peak-to-valley difference, imposing a great challenge to the reliable operation of distribution systems under cold climates. The objective of this paper is to establish a distributionally robust demand response (DR) model for building energy systems for suppressing peak-to-valley load ratios by exploiting cooperative complementarity and flexible transformation characteris-tics of various household appliances. The thermodynamic effect of buildings is modeled for harvesting intermittent renewable energy sources (RESs) on the building roof in the form of thermal energy storages to reduce RES curtailments and eliminate thermal comfort violations in cold weather. Furthermore, the Wasserstein metric is adopted to develop the ambiguity set of the uncertainty probability distributions (PDs) of RESs, and thus, only historical data of RES output is needed rather than prior knowledge about the actual PDs. Finally, a computationally tractable mixed-integer linear programming reformulation is derived for the original distributionally robust optimization (DRO) model. The proposed DRO-based DR strategy was performed on multiple buildings over a 24 h scheduling horizon, and comparative studies have validated the effectiveness of the proposed strategy for building energy systems in reducing the peak/valley ratio and decreasing operation costs.

Keywords: building energy system; demand response; distributionally robust optimization; cold climate; rooftop solar photovoltaic

1. Introduction

1.1. Motivation

Building energy systems with various household appliances and distributed renewables have emerged as the predominant energy consumer and contributor to carbon emissions [1,2]. It is reported by the International Energy Agency (IEA) that the operations of building energy systems contributed to one-third of global electricity consumption and 26% of global CO_2 emissions, with an average growth rate of 1% per year in the past decade [3]. During cold weather conditions, the demand for electricity surges due to energy-intensive appliances like air conditioning units, electric heaters, and heat pumps in buildings [4]. The synchronization of energy-consuming activities among multiple buildings, such as simultaneously increasing their heating load, can result in an instantaneous surge in electricity demand, leading to a rapid escalation in peak loads in urban distribution systems [5]. In general, multiple buildings are supplied by a transformer with a rated capacity.

However, the frequent occurrence of transformer overloading under cold climates, caused by the rapid growth in electricity demand for heating, accelerates the insulation aging of the transformer and may even lead to power outages and disrupt the power supply to buildings [6]. The transformer overloading poses a significant threat to the reliability of power supply to building energy systems under cold climates [7]. Recent advancements in

smart meters, electric vehicles, air conditioners, heat pumps, and other smart appliances offer substantial load flexibility for building energy management. Therefore, demand-side response measures can help mitigate the peak load on distribution systems. Demand response (DR) is regarded as a primary approach for flattening the peak load curve of distributed systems by coordinating load shifting and shedding [8].

Furthermore, the integration of renewable energy sources, such as wind turbines and solar panels, within buildings offers a complementary approach to reduce reliance on urban distributed systems during peak demand periods [9]. Building rooftops have consistently been identified as desirable locations for photovoltaic (PV) system installations. Presently, approximately half of the total solar PV capacity additions are attributed to solar PV installations on buildings, including rooftops, and this proportion is projected to more than double by 2030 [10]. Large-scale decentralized PV electricity generation on building rooftops presents a promising alternative for supplying electricity to heating loads during cold weather, effectively reducing the net load of urban distributed systems. Nevertheless, solar generation on the building rooftops directly depends on sunlight availability, which fluctuates throughout the day due to varying weather conditions [11]. The intermittent nature of solar generation can lead to sudden changes in power output, posing challenges in maintaining a reliable electricity supply to buildings [12]. In this regard, the uncoordinated operation of heating appliances and the uncertainty in renewable energy resources represent critical concerns for ensuring a reliable and resilient power supply to buildings, particularly during peak hours under cold climates. Therefore, it is imperative to develop capable modeling and analysis methods for the synergistic energy management of building energy systems in cold climates, considering the uncertainty in the generation of rooftop solar PVs.

1.2. Literature Review

Existing DR programs for buildings are categorized into incentive-based DR and price-based DR [8,13,14]. The incentive-based DR, alternatively referred to as "system-led" or "emergency-based" DR programs, aims to incentivize customers to reduce and shift the energy consumption of electrical appliances for buildings by providing incentive payments during periods of stress [13]. Incentive-based DR programs include direct-load controls, interruptible tariffs, demand-bidding programs, and emergency programs. The price-based DR, also identified as "market-led" or "economic-based" DR programs, encourages customers to individually adjust their energy consumption from peak hours to less congested hours via time-varying power price signals [15]. In typical price-based DR programs, the electricity price can vary either at pre-set times or dynamically based on the time, and the types of electricity prices consist of time-of-use pricing, critical-peak price, and real-time price [8]. Due to the requirement for customers to commit to load reduction during the execution time of incentive-based DR programs, the incentive-based DR is more favorable than the price-based DR to effectively mitigate emergency peak loads during cold days [4,6]. Over 90% of DR load reduction schemes in the DR market have been implemented in recent years by diverse incentive-based DR programs, which have brought significant benefits for electric utilities and customers [16].

Numerous researchers have been engaged in modeling and simulating building flexibility resource systems from the demand and supply sides in power systems. Demand-side flexibility resources are commonly categorized into non-thermostatic loads, such as lights and thermostatic loads, including air-conditioning units [4]. In references [1,8] and [17], smart appliances like washing machines, dishwashers, and tumble dryers have been modeled to operate automatically at the optimal time set by consumers. The charging of smart electric vehicles (EVs) can be dynamically curtailed or delayed from times of high network load to nighttime with sophisticated technology, which can autonomously monitor and react to urban low-voltage distribution networks [18]. These features facilitate the adoption of more dynamic forms to the DR of buildings, ensuring enhanced support for the secure operation of electricity networks. To ensure energy efficiency and implement DR programs, building energy models have been consistently valuable tools in aiding the prediction and

management of building energy [4]. Statistically based machine learning models, such as artificial neural network models, have been used to forecast buildings' energy consumption [19]. However, the major limitation of the machine learning models is that the models need vast amounts of actual statistical data to train and cannot provide a detailed physical understanding. To overcome this drawback, a simplified thermal dynamics model was developed in [20] to simulate potential flexibility in residential and small commercial buildings. A more complicated resistance–capacitance model is proposed in [21] to calculate the thermostatic loads in a one-zone building. Nonetheless, these works failed to account for modeling and utilizing buildings' thermodynamic effects for harvesting intermittent renewable energy sources.

Optimal building DR strategies with different electric appliances and EVs have been extensively studied and reported in [22–25]. The DR strategies have been proposed in [22] to adjust temperature setpoints of HVAC systems for the peak load reduction of urban distribution networks. Two aggregate community-level DR strategies were developed in [23] to utilize the potential flexibility of the battery-switching EVs for peak shaving. In [24], a three-layer game theoretic-based strategy was proposed for coordinating smart buildings, EV fleets, and microgrids. In addition, different climate zones and building types can affect the building's physical and office workers' behavior in buildings. Both are considered in the DR strategies to balance electricity supply and demand in buildings. A real-time DR strategy based on deep reinforcement learning is proposed in [25] to jointly optimize home appliance schedules. Although many building DR strategies have been conducted in previous studies, earlier works merely focused on the different amounts of energy flexibility derived from heterogeneous building energy systems for supporting the operation of power distribution networks under cold climates. Additionally, the uncertainty in rooftop renewable generations has yet to be considered.

Various methods, such as robust optimization, stochastic programming, and distributionally robust optimization (DRO), have been proposed in the literature to handle the uncertainties effectively [26]. In Ref. [27], bi-level stochastic programming was applied to coordinate uncertain renewable generations and DR, where the generation uncertainty of wind turbine and photovoltaic was represented by a group of scenarios. In [28], a chance-constrained two-stage stochastic program was developed to minimize building energy costs where the uncertainties of the electricity prices, solar power generation, and weather conditions were represented by a versatile probability distribution. In [29], an effective chance-constrained cooperative operation strategy was proposed to enhance the profits of the multi-agent energy system and participating agents under uncertainties of the outdoor environment. Nevertheless, the accurate probability distribution of random variables is typically unknown, and the available historical data are scant [30]. On the contrary, in [31], the robust optimization method was adopted for the economic operation of the integrated energy system, considering thermal comfort and DR. A novel bilayer coordinated operation method was developed in [32] for the economic operations of the multi-energy building microgrid based on robust optimization. Nevertheless, since the robust optimization method only optimizes the objective for the worst-case scenarios, the method inevitably yields an excessively conservative outcome. The recently emerged DRO methods offer a superior alternative to stochastic and robust optimization methods, effectively addressing the susceptibility of stochastic programming and the insensitivity of robust optimization to probabilistic information [33,34].

1.3. Contribution

This paper proposes a data-driven DRO model that accounts for the uncertainty in the generation of rooftop solar PV to address the optimal DR problem of building energy systems under cold climate conditions. Considering buildings' thermal energy storage ability, an optimal DR strategy for heterogeneous households' appliances is proposed to reduce the peak/valley ratio, accommodate rooftop PV, and decrease operation costs. A comprehensive description of the thermal energy transfer process and its relationship

with temperature variations is provided. A data-driven Wasserstein-metric-based DRO is formulated to minimize operation costs considering the uncertainty in rooftop PVs, and then a mixed-integer linear programming reformulation of the original DRO mode is derived for computational tractability. The main contributions of this paper are threefold:

(1) An optimal DR strategy of schedulable household appliance loads, including HVACs, curtailable loads, and transferable loads, is proposed to ensure the consumers' comfortable temperature needs. By leveraging the complementarity and flexibility of loads in building energy systems and taking advantage of the thermal inertia of buildings, the proposed strategy can effectively reduce the curtailment of uncertain rooftop PV generation, decrease the peak-to-valley load ratio, and improve the economic performance of building energy systems.

(2) A detailed thermal resistor–capacitor model is established to accurately describe buildings' thermal dynamic characteristics, and the building thermodynamic effect is used in the renewable utilization process for harvesting intermittent rooftop PV generations in the form of thermal storage. The solar radiation and thermal energy interaction between indoor space and cold external environment through envelope structures are considered. This model provides a foundation for the efficient operation of building energy systems.

(3) The optimal DR problem of heterogeneous building energy systems is formulated as a data-driven DRO-based DR mode to handle the inherent uncertainty in the generation of rooftop solar PV. The Wasserstein metric is employed to construct the ambiguity, which only requires historical data of rooftop PV generations rather than actual probability distributions. Furthermore, an equivalent mixed-integer linear programming reformulation of the original DRO model is derived for computational tractability.

2. Optimization-Based Demand Response of Heterogeneous Building Energy Systems

2.1. Optimal Demand Response Framework of Buildings

This study aims to investigate the optimal DR problem of building energy systems under cold climates, and an aggregator is incorporated to coordinate and manage the energy usage of different electrical loads within these building energy systems. Figure 1 depicts the aggregation of energy systems equipped with rooftop solar PVs and different types of electrical loads of household appliances. Here, the appliances of buildings can be divided into four load categories: curtailable loads, transferrable loads, HVACs, and base loads [10,16]. The communication and control for flexible loads are performed with the aggregator via the energy management system [1]. Given that the electrical energy fed back to the power grid needs to meet the quality requirements, this study does not consider the sale of electricity from building energy systems to the power grid. Under cold climates, the increased thermal demand from consumers and the volatility of rooftop PV generation pose challenges to the efficient energy management of buildings. Uncertainty in rooftop PV generation can lead to difficulties in designing operational strategies, resulting in rapid load rate changes and potential overloading of transformers. This can negatively impact the stability of power grids and the economic performance of buildings. The thermal storage characteristics of buildings offer an effective means to fulfill consumers' thermal comfort requirements and mitigate PV fluctuations under cold climates. By fully utilizing the thermal energy storage capability of buildings and coordinating with flexible load scheduling such as HVAC, curtailable loads, and transferable loads, the curtailment of renewable energy, the peak/valley ratio, and the violation of consumers' thermal comfort can all be reduced. Therefore, an optimal DR strategy considering uncertain rooftop PV is proposed to coordinate and optimize the load transfer amount and curtailment along with HVAC operations to coordinate the usage of the flexible loads and reduce economic costs.
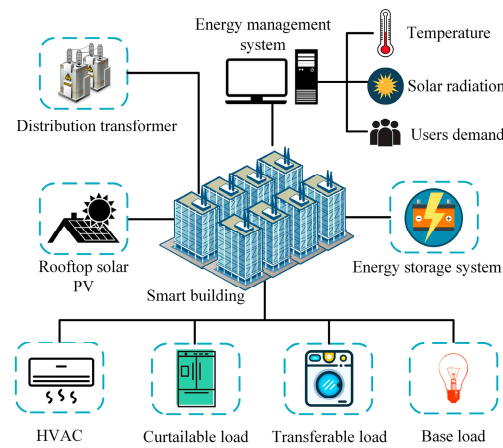
Figure 1. Framework of demand response in heterogeneous building energy systems.

To realize the optimal operation of the building energy system, the method adopted in this paper is the scheduling of flexible resources, including curtailable loads, transferable loads, HVACs, and the ESS. And the basic principle of scheduling is to shift power purchases from the grid as far as possible to the low-price periods, which can improve the economy of the building energy system. However, the uncertainty of rooftop PV makes scheduling more difficult. Therefore, DRO is introduced to handle the challenge. Then, by solving the DRO model, the optimal strategy of the building energy system is obtained.

2.2. Building Energy System Modeling

2.2.1. Curtailable Loads and Transferable Loads

To fully tap into the responsiveness potential of buildings, it is necessary to construct models for curtailable loads and transferable loads [35]. Curtailable loads mean the loads whose electrical power can be curtailed to a certain extent. Transferable loads mean the loads that can transfer part of the power to the other time slots, but the total power during the scheduling periods must remain unchanged. Obviously, the adjustment of curtailable loads and transferable loads will bring discomfort to consumers [17]. Therefore, reasonable subsidies should be paid to the consumers to compensate for their sacrifices. According to the above characteristics, the DR loads, including curtailable loads and transferable loads, are modeled as follows:

$$L_t^{\mathrm{DR}} = L_t^{\mathrm{ori}} - L_t^{\mathrm{tran,out}} + L_t^{\mathrm{tran,in}} - L_t^{\mathrm{cut}} \tag{1}$$

$$\sum_{t \in T} L_t^{\mathrm{tran,out}} = \sum_{t \in T} L_t^{\mathrm{tran,in}} \tag{2}$$

$$L_t^{\mathrm{tran,out}} L_t^{\mathrm{tran,in}} = 0 \tag{3}$$

$$0 \le L_t^{\mathrm{cut}} \le L_{\max}^{\mathrm{cut}} \tag{4}$$

$$0 \le L_t^{\mathrm{tran,out}}, L_t^{\mathrm{tran,in}} \le L_{\max}^{\mathrm{tran}} \tag{5}$$

where the subscript t means time slot t; L_t^{DR} and L_t^{ori} are original electrical loads and actual loads after DR; $L_t^{\mathrm{tran,in}}$ is the electrical loads that transferred into time slot t; L_t^{cut} and $L_t^{\mathrm{tran,out}}$ are the loads reduced and transferred out of the time slot t, respectively; $L_{\max}^{\mathrm{cut}}$ and $L_{\max}^{\mathrm{tran}}$ are maximum values of reduced load and transferred load, respectively. Equation (1) shows the electrical loads after adjusting reduced loads and transferable loads. Equation (2) makes sure the total value of transferred loads remains unchanged during the whole scheduling period. Equation (3) means loads cannot be transferred out of and into the same time slot. Equations (4) and (5) constrain the upper and lower limits of reduced loads and transferred loads.

2.2.2. HVAC

As a temperature control load, HVACs can convert electrical energy into thermal energy, and this is one of the main ways to provide heat sources for indoor consumers in cold climates [22]. Due to the low sensitivity of the human body to temperature and the thermal inertia of buildings, HVAC can be used to participate in DR while ensuring a comfortable temperature range for consumers. The change in its operating power affects the electric load and thermal load [28]. The electrical power of HVAC can be divided into two parts, which are shown below:

$$P_t^{\text{HVAC}} = P_t^{\text{thermal}} + P_t^{\text{fan}} \tag{6}$$

where P_t^{thermal} and P_t^{fan} are the heating power and fan power of HVAC, respectively; P_t^{HVAC} is the total power of HVAC equipment in a certain indoor room.

The thermal power and fan power of HVAC can be calculated by the following equations:

$$P_t^{\text{thermal}} = [m_{k,t}^{\text{room}} C_{\text{air}} (T_{k,t}^{\text{supply}} - T_{k,t}^{\text{room}})] / C_{\text{cop}} \tag{7}$$

$$P_t^{\text{fan}} = [m_{k,t}^{\text{room}} (P_{\text{static}} - \rho \frac{v^2}{2})] / (\eta_{\text{motor}} \eta_{\text{fan}}) \tag{8}$$

where $m_{k,t}^{\text{room}}$ is the air mass flow into or out to the room k; C_{air} and C_{cop} are the specific heat capacity of air and the performance coefficient of HVAC; $T_{k,t}^{\text{supply}}$ and $T_{k,t}^{\text{room}}$ are the supply of air temperature and indoor temperature in the room k; P_{static}, ρ, v are static pressure difference of HVAC, air density and wind speed, respectively; η_{motor} and η_{fan} are motor coefficient and fan coefficient of air supply equipment.

The constraints required for HVAC operations are as follows:

$$T_{\text{min}}^{\text{room}} \leq T_{k,t}^{\text{room}} \leq T_{\text{max}}^{\text{room}} \tag{9}$$

$$T_{\text{min}}^{\text{supply}} \leq T_{k,t}^{\text{supply}} \leq T_{\text{max}}^{\text{supply}} \tag{10}$$

$$\eta T_{\text{min}}^{\text{supply}} \leq T_{k,t+1}^{\text{supply}} - T_{k,t}^{\text{supply}} \leq \eta T_{\text{max}}^{\text{supply}} \tag{11}$$

where $T_{\text{max}}^{\text{room}}$ and $T_{\text{min}}^{\text{room}}$ are the upper and lower limit of consumers' comfortable temperature interval; $T_{\text{max}}^{\text{supply}}$ and $T_{\text{min}}^{\text{supply}}$ are the maximum and minimum values of HVAC's supply air temperature; η is the change rate coefficient for supply air temperature. Equation (9) considers the temperature demand of consumers and ensures the room temperature is within a comfortable range. Equations (10) and (11) limit the magnitude and change rate of HVAC's supply air temperature.

2.2.3. Thermal Dynamic Model of Buildings

The indoor space of buildings can be modeled by the resister–capacity network considering the thermodynamics of the buildings. In this model, an indoor room has five nodes, i.e., one room node and four wall nodes. Moreover, there is a window on one of the walls for each indoor room [2]. The heat can be transferred between nodes through thermal resistance and stored in nodes through thermal capacity [19].

According to the theory of thermodynamics, the heat energy will transfer from the indoor space of the building to the cold external environment through each side of the building envelope structures. Moreover, rooms can transfer heat with each other through walls. At the same time, solar radiation also has a great influence on the temperature of the building [4]. It can be assumed that all rooms in the building have the same envelope structures with the same parameters. Therefore, the HVAC loads of the whole building can be calculated by summing the HVAC power of all indoor rooms.

The mathematical model of the indoor room equipped with HVAC can be established as follows:

$$C_{ij}^{\text{wall}}\frac{dT_{ij}^{\text{wall}}}{dt} = \sum_{j \in N_{\text{wall}}} \frac{T_j - T_{ij}^{\text{wall}}}{R_{ij}^{\text{wall}}} + q_{ij}v_{ij}A_{ij}^{\text{wall}}Q_{ij}^{\text{rad}} \tag{12}$$

$$\begin{aligned}
C_k^{\text{room}}\frac{dT_k^{\text{room}}}{dt} = \quad & \sum_{j \in N_{\text{room}}} \frac{T_{ij}^{\text{wall}} - T_k^{\text{room}}}{R_{ij}^{\text{wall}}} + \pi_{ij}\sum_{j \in N_{\text{room}}} \frac{T_j - T_k^{\text{room}}}{R_{ij}^{\text{win}}} \\
& + Q_k^{\text{int}} + m_k^{\text{room}}C_{\text{air}}(T_k^{\text{supply}} - T_k^{\text{room}}) + \pi_{ij}w_{ij}A_{ij}^{\text{wall}}Q_{ij}^{\text{rad}}
\end{aligned} \tag{13}$$

where C_{ij}^{wall} and C_{ij}^{room} are thermal capacities of the walls and indoor rooms; T_{ij}^{wall} and T_j are wall temperatures and jth node's temperature; R_{ij}^{wall} and R_{ij}^{win} are thermal resistances of walls and windows; N_{wall} and N_{room} are the numbers of wall nodes and room nodes; q_{ij} and v_{ij} are sunlit wall identifiers and absorption coefficient of the walls; A_{ij}^{wall} and Q_{ij}^{rad} are the area of the wall and radiative heat flux density on the wall; π_{ij} and Q_k^{int} are sunlit window identifiers and internal heat gain; w_{ij} is transmittance coefficient of the window. If the wall ij is exposed to external solar radiation, q_{ij} equals 1; otherwise, it is taken as 0. If the wall ij has a window, π_{ij} equals 1; otherwise, it is taken as 0. Equation (12) describes the temperature variation pattern of wall nodes, and Equation (13) describes the temperature variation pattern of room nodes.

Considering an indoor area whose structure is shown in Figure 2, the above thermal balance model can be specifically converted into the following form:

$$C_{12,k}^{\text{wall}}(T_{12,k,t+1}^{\text{wall}} - T_{12,k,t}^{\text{wall}}) = \Delta t\left(\frac{T_{k,t}^{\text{room}} - T_{12,k,t}^{\text{wall}}}{R_{12,k}^{\text{wall}}} + \frac{T_{12,k,t}^{\text{adj}} - T_{12,k,t}^{\text{wall}}}{R_{12,k}^{\text{wall}}}\right) \tag{14}$$

$$C_{13,k}^{\text{wall}}(T_{13,k,t+1}^{\text{wall}} - T_{13,k,t}^{\text{wall}}) = \Delta t\left(\frac{T_{k,t}^{\text{room}} - T_{13,k,t}^{\text{wall}}}{R_{13,k}^{\text{wall}}} + \frac{T_{13,k,t}^{\text{adj}} - T_{13,k,t}^{\text{wall}}}{R_{13,k}^{\text{wall}}}\right) \tag{15}$$

$$C_{14,k}^{\text{wall}}(T_{14,k,t+1}^{\text{wall}} - T_{14,k,t}^{\text{wall}}) = \Delta t\left(\frac{T_{k,t}^{\text{room}} - T_{14,k,t}^{\text{wall}}}{R_{14,k}^{\text{wall}}} + \frac{T_{14,k,t}^{\text{out}} - T_{14,k,t}^{\text{wall}}}{R_{14,k}^{\text{wall}}} + q_{14,k}v_{14,k}A_{14,k}^{\text{wall}}Q_{14,k,t}^{\text{rad}}\right) \tag{16}$$

$$C_{15,k}^{\text{wall}}(T_{15,k,t+1}^{\text{wall}} - T_{15,k,t}^{\text{wall}}) = \Delta t\left(\frac{T_{k,t}^{\text{room}} - T_{15,k,t}^{\text{wall}}}{R_{15,k}^{\text{wall}}} + \frac{T_{15,k,t}^{\text{out}} - T_{15,k,t}^{\text{wall}}}{R_{15,k}^{\text{wall}}} + q_{15,k}v_{15,k}A_{15,k}^{\text{wall}}Q_{15,k,t}^{\text{rad}}\right) \tag{17}$$

$$\begin{aligned}
C_k^{\text{room}}(T_{k,t+1}^{\text{room}} - T_{k,t}^{\text{room}}) = \quad & \Delta t\Bigg[\sum_{j=1}^{4} \frac{T_{1j,k,t}^{\text{wall}} - T_{k,t}^{\text{room}}}{R_{1j,k}^{\text{wall}}} + \frac{T_{k,t}^{\text{out}} - T_{k,t}^{\text{room}}}{R_{15,k}^{\text{win}}} + Q_k^{\text{int}} \\
& + m_{k,t}^{\text{room}}C_{\text{air}}(T_{k,t}^{\text{supply}} - T_{k,t}^{\text{room}}) + w_{15,k}A_{15,k}^{\text{wall}}Q_{k,t}^{\text{rad}}\Bigg]
\end{aligned} \tag{18}$$

where $T_{ij,k,t}^{\text{out}}$ and $T_{ij,k,t}^{\text{adj}}$ are the outdoor temperature and adjacent node temperature; Δt is the scheduling interval. The above equations show the relationship between wall temperatures and room temperatures between two time slots. Based on the comfort demand of building consumers and electrical power demand, this model can flexibly schedule the HVAC power to realize the optimal operation with the help of building thermal inertia. Accumulating all HVAC powers in the entire building can obtain the total power which can be intelligently regulated as a flexible load aggregation.
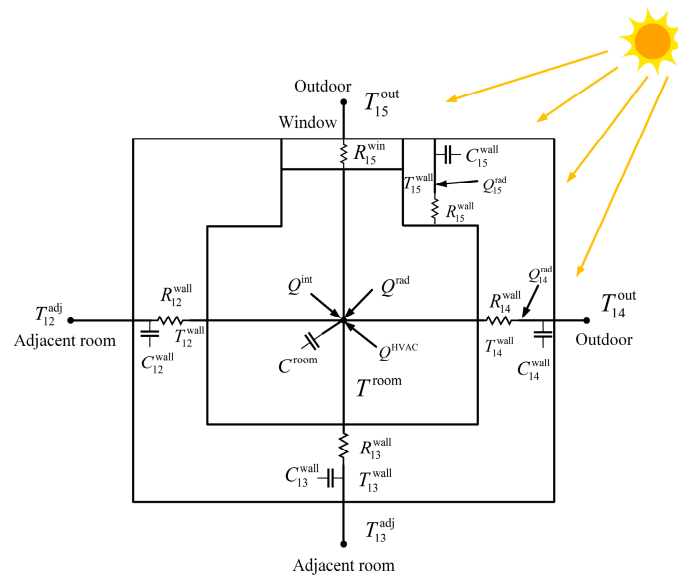
Figure 2. Schematic diagram of the resistor–capacity network model for a room.

2.2.4. Energy Storage System

ESS is helpful in dealing with the uncertainty of PV and the changes in power price [13]. Therefore, the following ESS model is established.

$$S_{t+1}^{\text{ESS}} = S_t^{\text{ESS}} + (P_{\text{C},t}^{\text{ESS}} \eta_{\text{C}}^{\text{ESS}} - P_{\text{D},t}^{\text{ESS}} / \eta_{\text{D}}^{\text{ESS}}) / E_{\text{ESS}} \tag{19}$$

$$S_1^{\text{ESS}} = S_T^{\text{ESS}} \tag{20}$$

$$P_{\text{C},t}^{\text{ESS}} P_{\text{D},t}^{\text{ESS}} = 0 \tag{21}$$

$$0 \le P_{\text{C},t}^{\text{ESS}} \le P_{\text{C,max}}^{\text{ESS}} \tag{22}$$

$$0 \le P_{\text{D},t}^{\text{ESS}} \le P_{\text{D,max}}^{\text{ESS}} \tag{23}$$

$$S_{\text{min}}^{\text{ESS}} \le S_t^{\text{ESS}} \le S_{\text{max}}^{\text{ESS}} \tag{24}$$

where S_t^{ESS} and E_{ESS} are the SOC and energy capacity of ESS; $P_{\text{C},t}^{\text{ESS}}$ and $P_{\text{D},t}^{\text{ESS}}$ are charging and discharging power of ESS; $\eta_{\text{C}}^{\text{ESS}}$ and $\eta_{\text{D}}^{\text{ESS}}$ are charging and discharging efficiency; $P_{\text{C,max}}^{\text{ESS}}$ and $P_{\text{D,max}}^{\text{ESS}}$ are the maximum values of charging and discharging power; $S_{\text{max}}^{\text{ESS}}$ and $S_{\text{min}}^{\text{ESS}}$ are the maximum and minimum values of ESS's SOC. Equation (19) shows the SOC change due to charging and discharging behaviors. Equation (20) maintains the periodic operation of ESS. Equation (21) ensures charging and discharging do not occur simultaneously. Equations (22) and (23) restrict the upper and lower limits of charging power and discharging power. Equation (24) limits the energy stored in the ESS within a reasonable capacity range at all times.

2.2.5. Power Balance

Therefore, considering the electrical power balance of the whole building [20], the following equation is put forward:

$$P_t^{\text{HVAC}} + L_t^{\text{DR}} + P_{\text{C},t}^{\text{ESS}} = P_t^{\text{PV}} + P_t^{\text{buy}} + P_{\text{D},t}^{\text{ESS}} \tag{25}$$

$$0 \le P_t^{\text{buy}} \le P_{\text{max}}^{\text{buy}} \tag{26}$$

where P_t^{buy} is the purchased power from the grid and P_t^{PV} is the output of PV installed on the roof of the buildings; $P_{\text{max}}^{\text{buy}}$ is the maximum value of purchased power from the grid.

Equation (25) is the balanced relationship among various powers in the building energy systems. Equation (26) restricts the amount of purchased power from the grid.

2.3. Data-Driven Distributionally Robust Demand Response Optimization Model Formulation

For a building energy system, the operation economy is usually the primary focus. Thus, the objective function of the optimization schedule is shown as Equation (27), which can be divided into two terms. The first term C_t^{DR} refers to the economic subsidies for consumers to participate in DR, which can compensate for the negative impact of curtailing and transferring loads on the power supply satisfaction. It is associated with the decisions that are independent of the uncertainty. The second term C_t^{grid} refers to the expected fees that need to be paid for purchasing power from the grid affected by the imposed uncertainty considering the worst-case realization of the probability distributions.

$$\min C = \sum_{t \in T} \left\{ C_t^{\text{DR}} + \sup_{\mathbb{P} \in \hat{P}} \mathbb{E}_{\mathbb{P}} \left[\inf C_t^{\text{grid}} \right] \right\} \tag{27}$$

where C is the total cost of building energy system, and T is the set of time slots; $\hat{P}$ is the ambiguity set that contains the possible distributions of P_t^{PV}.

$$C_t^{\text{DR}} = \varphi_{\text{tran}} L_t^{\text{tran,out}} + \varphi_{\text{cut}} L_t^{\text{cut}} \tag{28}$$

$$C_t^{\text{grid}} = \lambda_t^{\text{buy}} P_t^{\text{buy}} \tag{29}$$

where λ_t^{buy} is the price for purchasing power from the grid; φ_{tran} and φ_{cut} are the subside price for transferable loads and reduced loads.

In summary, the data-driven DRO-based DR model of building energy systems can be compactly formulated as follows:

$$\begin{cases} \min C = \sum_{t \in T} \left\{ C_t^{\text{DR}}(\boldsymbol{x}_t) + \sup_{\mathbb{P} \in \hat{P}} \mathbb{E}_{\mathbb{P}} \left[\inf C_t^{\text{grid}}(\boldsymbol{y}_t) \right] \right\} \\ \text{over } \boldsymbol{x} := \left\{ L_t^{\text{tran,out}}, L_t^{\text{tran,in}}, L_t^{\text{cut}}, T_{k,t}^{\text{supply}}, P_{\text{C},t}^{\text{ESS}}, P_{\text{D},t}^{\text{ESS}} \right\}_{t \in T} \\ \quad \boldsymbol{y} := \left\{ P_t^{\text{buy}} \right\}_{t \in T} \\ \text{s.t. } \boldsymbol{x} \in \mathcal{X} \\ \quad \boldsymbol{T}(\boldsymbol{x}) \hat{\boldsymbol{P}}^{\text{PV}} + \boldsymbol{h}(\boldsymbol{x}) \leq \boldsymbol{W} \boldsymbol{y} \end{cases} \tag{30}$$

where $\mathcal{X}$ is the feasible region of $\boldsymbol{x}$; $\boldsymbol{T}(\boldsymbol{x})$, $\boldsymbol{h}$, and $\boldsymbol{W}$ are parameter matrices or vectors obtained from constraints (1)–(11) and (14)–(26); and $\hat{\boldsymbol{P}}^{\text{PV}}$ is a random matrix comprising the uncertain parameters of rooftop PV generation.

3. Solution Methodology of Distributionally Robust Demand Response Problem

3.1. Linearization of Bi-Linear Terms

In the constructed models, Equations (3) and (21) are nonlinear constraints. The following method can be leveraged to transform such constraints [33]. After processing, Equations (3) and (5) could be merged and converted into Equations (31) and (32). Equations (21)–(23) could be merged and converted into Equations (33) and (34).

$$0 \leq L_t^{\text{tran,out}} \leq \gamma_t^{\text{tran}} L_{\max}^{\text{tran}} \tag{31}$$

$$0 \leq L_t^{\text{tran,in}} \leq (1 - \gamma_t^{\text{tran}}) L_{\max}^{\text{tran}} \tag{32}$$

$$0 \leq P_{\text{C},t}^{\text{ESS}} \leq \gamma_t^{\text{ESS}} P_{\text{C},\max}^{\text{ESS}} \tag{33}$$

$$0 \leq P_{\text{D},t}^{\text{ESS}} \leq (1 - \gamma_t^{\text{ESS}}) P_{\text{D},\max}^{\text{ESS}} \tag{34}$$

where γ_t^{tran} and γ_t^{ESS} are introduced binary variables.

3.2. Construction of Wasserstein Metric-Based Ambiguity Set

It is necessary to obtain the probability to calculate the expectation value of random P_t^{PV}. However, it is difficult to obtain the actual probability distribution, and only a set of historical samples $\hat{P}^{\text{PV}} = \left\{ \hat{P}_1^{\text{PV}}, \hat{P}_2^{\text{PV}}, \ldots, \hat{P}_N^{\text{PV}} \right\}$ is available, where N is the sample number. The Wasserstein metric is leveraged to construct the ambiguity set $\hat{\mathbb{P}}_N$. According to the historical data, an empirical probability distribution $\hat{\mathbb{P}}_N = \frac{1}{N}\sum_{i=1}^{N} \delta_{\hat{P}_i^{\text{PV}}}$ can be derived to estimate the actual probability distribution, and $\delta_{\delta_{\hat{P}_i^{\text{PV}}}}$ is the Dirac measure of the historical sample $\hat{P}_i^{\text{PV}}$ [36]. As shown in Equation (35), the distance between the actual probability distribution and estimated probability distribution can be calculated as follows:

$$W(\hat{\mathbb{P}}_N, \mathbb{P}) = \inf_{\Pi}\left\{ \int_{\Xi^2} \|\omega - \hat{\omega}\| \Pi(d\omega, d\hat{\omega}) \right\} \tag{35}$$

where Ξ is the compactor support of the random variable; Π is a joint distribution of ω and $\hat{\omega}$ with marginal probability distribution $\hat{\mathbb{P}}_N$ and $\mathbb{P}$. Then, we can construct the ambiguity set as Equation (36):

$$\hat{\mathbb{P}} := \{W(\hat{\mathbb{P}}_N, \mathbb{P}) \le \varepsilon(N)\} \tag{36}$$

where $\varepsilon(N)$ is the radius of the ambiguity set $\hat{\mathbb{P}}$ and the center is $\hat{\mathbb{P}}_N$, which is a function of the confidence level β and the sample number N, as follows:

$$\varepsilon(N) = D\sqrt{\frac{2}{N}\ln(\frac{1}{1-\beta})} \tag{37}$$

where D is the diameter of the support of random variable [36].

3.3. Reformulation of Data-Driven DRO Model

In general, a two-stage distributionally robust linear programming model can be compactly formulated as

$$\begin{aligned} &\min \mathbf{c}^\top \mathbf{x} + \mathcal{Z}(\mathbf{x}) \\ &\text{s.t. } \mathbf{x} \in \mathcal{X} \end{aligned} \tag{38}$$

where

$$\mathcal{Z}(\mathbf{x}) = \sup_{\mathbb{P} \in \hat{\mathcal{P}}} \mathbb{E}_{\mathbb{P}}[Z(\mathbf{x}, \widetilde{\boldsymbol{\xi}})]. \tag{39}$$

Here, $\mathcal{X} \in \mathbb{R}^{N_1}$ is the feasible set of the here-and-now decisions $\mathbf{x}$, $\mathbf{c}$ is the coefficient vector of $\mathbf{x}$, $\mathcal{Z}(\mathbf{x})$ is the worst-case expected wait-and-see cost, $\widetilde{\boldsymbol{\xi}} \subseteq \mathbb{R}^{K}$ is a random vector, whose distribution $\mathbb{P}$ is supported on Ξ, $\hat{\mathcal{P}}$ is an ambiguity set that contains the possible distributions of $\widetilde{\boldsymbol{\xi}}$, and $Z(\mathbf{x}, \boldsymbol{\xi})$ is a recourse function that constitutes the optimal value of the parametric linear recourse problem, that is

$$\begin{aligned} Z(\mathbf{x}, \boldsymbol{\xi}) = \inf \; &(\mathbf{Q}\boldsymbol{\xi} + \mathbf{q}^\top)\mathbf{y} \\ \text{s.t. } &\mathbf{y} \in \mathbb{R}^{N_2} \\ &\mathbf{A}(\mathbf{x})\boldsymbol{\xi} + \mathbf{b}(\mathbf{x}) \le \mathbf{W}\mathbf{y}. \end{aligned} \tag{40}$$

where $\mathbf{y}$ is the wait-and-see decisions; $\mathbf{A}(\mathbf{x})$ and $\mathbf{b}(\mathbf{x})$ are matrix- and vector-valued affine functions, respectively; $\mathbf{Q}$, $\mathbf{W}$, and $\mathbf{q}$ are parameter matrices or vectors with appropriate dimensionality.

In general, the true distribution of $\widetilde{\boldsymbol{\xi}}$ is unknown, and I samples of $\widetilde{\boldsymbol{\xi}}$, i.e., $\hat{\boldsymbol{\xi}}_1, \ldots, \hat{\boldsymbol{\xi}}_I$, can be obtained from history data. Define $[\bullet]$ as the index set $\{1, 2, \ldots, \bullet\}$. Let $\mathbb{R}_+$ denote the set of non-negative reals and ϵ denote the Wasserstein ball of radius. According to Ref. [37], when $\mathbf{Q} = 0$ and the ambiguity set is constructed using the 1-Wasserstein metric with

reference distance $d(\boldsymbol{\xi}_1, \boldsymbol{\xi}_2) = \|\boldsymbol{\xi}_1 - \boldsymbol{\xi}_2\|_1$, problem (38) can be equivalently transformed into the following tractable linear model:

$$
\begin{aligned}
\min \quad & \epsilon\lambda + \frac{1}{I}\sum_{i\in[I]} \boldsymbol{q}^\top \boldsymbol{y}_i \\
\text{s.t.} \quad & \boldsymbol{x} \in \mathcal{X}, \boldsymbol{\lambda} \in \mathbb{R}_+, \boldsymbol{y}_i \in \mathbb{R}^{N_2} \ \forall i \in [I] \\
& \boldsymbol{\phi}_k \in \mathbb{R}^{N_2}, \boldsymbol{\varphi}_k \in \mathbb{R}^{N_2} \ \forall k \in [K] \\
& \boldsymbol{A}(\boldsymbol{x})\hat{\boldsymbol{\xi}}_i + \boldsymbol{b}(\boldsymbol{x}) \le \boldsymbol{W}\boldsymbol{y}_i \ \forall i \in [I] \\
& \boldsymbol{q}^\top \boldsymbol{\phi}_k \le \lambda, \ \boldsymbol{q}^\top \boldsymbol{\varphi}_k \le \lambda \ \forall k \in [K] \\
& \boldsymbol{A}(\boldsymbol{x})\boldsymbol{e}_k \le \boldsymbol{W}\boldsymbol{\phi}_k, -\boldsymbol{A}(\boldsymbol{x})\boldsymbol{e}_k \le \boldsymbol{W}\boldsymbol{\varphi}_k \ \forall k \in [K]
\end{aligned}
\tag{41}
$$

where $\boldsymbol{e}_k$ is the vector of all ones, and $\boldsymbol{\phi}_k$ and $\boldsymbol{\varphi}_k$ are auxiliary variables.

Based on the above transformation, the proposed DRO-based DR model based on the Wasserstein metric can be recast into the following computationally tractable form:

$$
\begin{aligned}
\min \quad & \varepsilon(N)\lambda + \frac{1}{|N|}\sum_{i=1}^{N} \boldsymbol{q}^{\mathrm{T}} \boldsymbol{y}_i \\
\text{s.t.} \quad & \boldsymbol{x} \in \mathcal{X}, \lambda \in \mathbb{R}_+, \boldsymbol{y}_i \in \mathbb{R}^{T} \ \forall i \in [N] \\
& \boldsymbol{\phi}_k \in \mathbb{R}^{T}, \boldsymbol{\varphi}_k \in \mathbb{R}^{T} \ \forall k \in [K^{\mathrm{PV}}] \\
& \boldsymbol{T}(\boldsymbol{x})\hat{\boldsymbol{P}}_i^{\mathrm{PV}} + \boldsymbol{h}(\boldsymbol{x}) \le \boldsymbol{W}\boldsymbol{y}_i \ \forall i \in [N] \\
& \boldsymbol{q}^{\mathrm{T}} \boldsymbol{\phi}_k \le \lambda, \ \boldsymbol{q}^{\mathrm{T}} \boldsymbol{\varphi}_k \le \lambda \ \forall k \in [K^{\mathrm{PV}}] \\
& \boldsymbol{T}(\boldsymbol{x})\boldsymbol{e}_k \le \boldsymbol{W}\boldsymbol{\phi}_k, -\boldsymbol{T}(\boldsymbol{x})\boldsymbol{e}_k \le \boldsymbol{W}\boldsymbol{\varphi}_k \ \forall k \in [K^{\mathrm{PV}}]
\end{aligned}
\tag{42}
$$

where K^{PV} is the dimensionality of $\hat{\boldsymbol{P}}_i^{\mathrm{PV}}$ and $\boldsymbol{q}$ is a parameter vector obtained from (29). Off-the-shelf commercial solvers can be used to readily solve (42) with reliable accuracy.

In summary, the modeling and transforming procedure of the paper is shown in Figure 3.
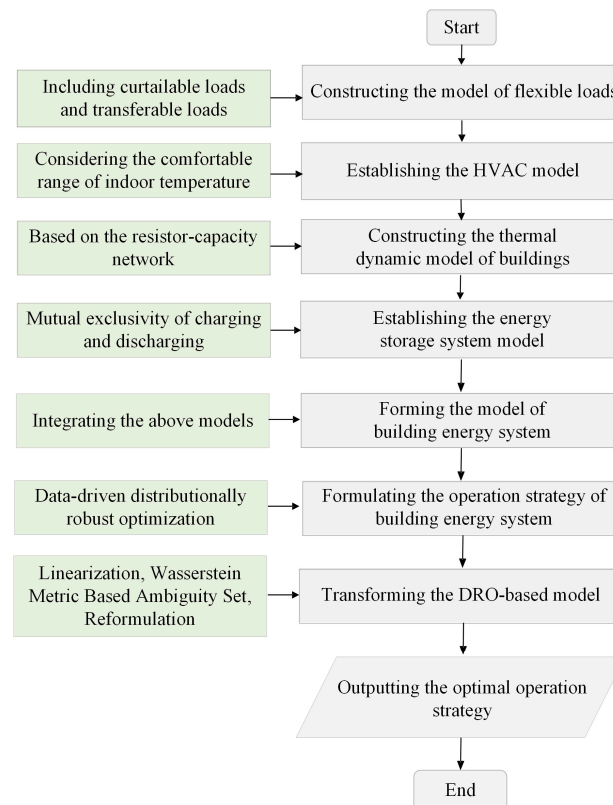

Figure 3. Flowchart of modeling and transforming procedure.
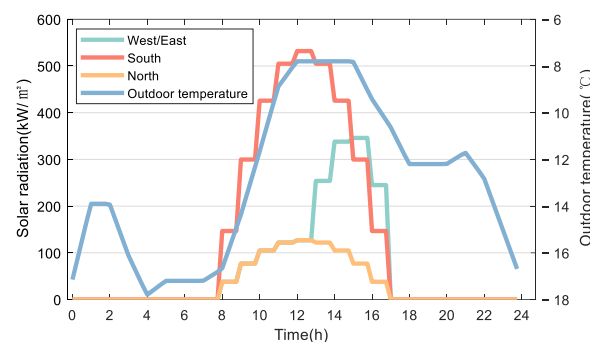
4. Results

This section verifies the effectiveness of the proposed strategy through the case study. Based on the heating application circumstances in cold weather, operation effects under different operating modes are compared. The optimization problem is solved in the Matlab R2023a platform. The hardware environment of the PC is Intel (R) Core (TM) i7-10700K CPU @ 3.80 GHz with 32 GB RAM.

4.1. Case Setting

The optimization period is 24 h and Δt is 15 min. The indoor HVACs are continuously in operation. When heating or cooling the indoor area of a building, it takes some time to raise or lower the indoor temperature of the building, and the slow thermal behavior of the building promotes its thermal inertia. The comfortable temperature range for consumers depends on various environmental factors, such as temperature, metabolic rate, and airflow rate. Therefore, the comfortable temperature range that consumers can accept may vary depending on the situation. The preferred thermal neutral range for ordinary people is between 17 °C and 33 °C. In this paper, the comfortable temperature range for smart building consumers is set to 20 °C~24 °C. However, the proposed optimization strategy is not limited to the above range. By changing the control scheme of the HVACs, the strategy can be further applied to other hotter or colder climate areas. The building parameters and HVAC parameters are shown in Table 1. The solar radiation and outdoor temperature are shown in Figure 4. There are 8 smart buildings in this section and each building has 100 rooms. A total of 1000 PV original output curves are obtained according to historical data and then are reduced into 5 scenarios, which are shown in Figure 5. The curves of electrical loads and power prices are shown in Figure 6. The reduced load cannot exceed 10% of the load and the transferred load cannot exceed 30% of the load at each time slot. The maximum charging and discharging power of the ESS are 200 kW, and the energy capacity is 2000 kWh. The charging and discharging efficiency are both 0.95.

**Table 1.** Parameters of buildings and HVACs.

Building Parameters	Value	HVAC Parameters	Value
R^{wall}	0.06 K/W	ρ	1.29 kg/m^3
R^{wall} with a window	0.08 K/W	C_{air}	1005 J/kg·°C
R^{win}	0.02 K/W	v	4 m/s
C^{wall}	7.9×10^5 J/K	C_{cop}	3.0
C^{wall} with a window	2.6×10^7 J/K	P_{static}	135 Pa
C^{room}	2.5×10^5 J/K	$\eta_{\text{motor}} \cdot \eta_{\text{fan}}$	0.15

Figure 4. Solar radiation and outdoor temperature.
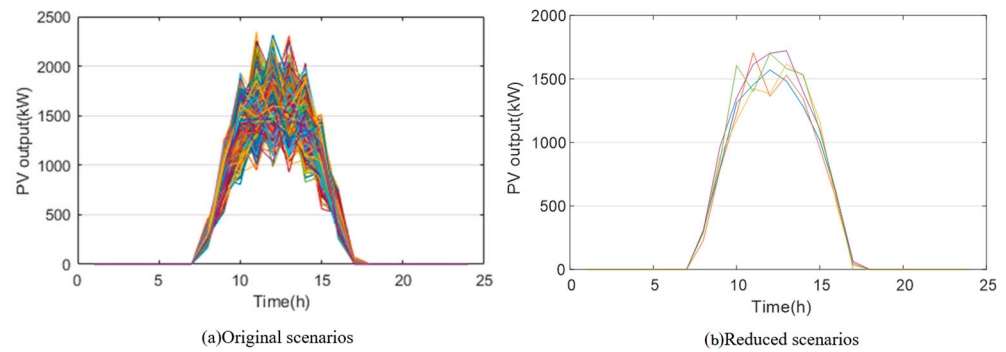
Figure 5. Original scenarios and reduced scenarios of PV.
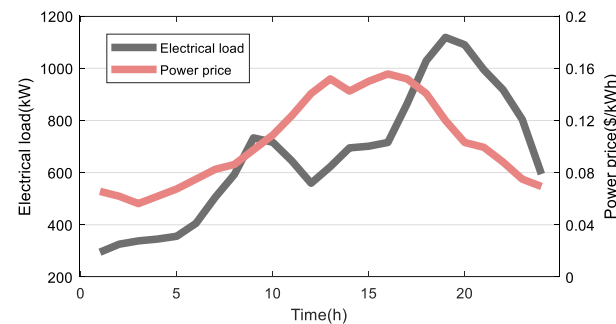
Figure 6. Original electrical loads and power price.

4.2. Results Analysis

To highlight the superiority of the proposed strategy, four cases are set to compare, whose differences are clarified in Table 2. In Case 1, the room temperature is set as a constant value rather than a range, and flexible loads are non-schedulable. In Case 2, the room temperature is still set as a constant value, but flexible loads are schedulable. In Case 3, the room temperature is considered a comfortable range for consumers, and flexible loads are non-schedulable. Case 4 is the proposed strategy with a comfortable temperature range and schedulable flexible loads.

Table 2. Differences among the four cases.

Case	Room Temperature	Flexible Load
1	Constant value	Non-schedulable
2	Constant value	Schedulable
3	Comfortable range	Non-schedulable
4	Comfortable range	Schedulable

The economy of different cases is shown in Table 3. Case 4 has the best economy, while Case 1 has the worst. Case 1 does not schedule flexible loads and utilize the thermal inertia of buildings to respond to the power price, so the payment to the grid for purchasing power is the highest. Case 2 gives full play to the flexible loads. The loads in peak periods of power price are curtailed or transferred to the valley periods, which can reduce the payment for purchasing power compared to Case 1. Case 3 utilizes the thermal storage characteristics of the buildings to flexibly adjust the HVAC power while meeting consumers' comfort needs. Therefore, the HVAC power in the peak period is reduced, which decreases the payment to the grid compared to Case 1. Case 4 combines the advantages of Case 2 and Case 3 while leveraging the regulation potential of curtailable loads, transferrable loads, and HVACs, maximizing the economy of smart buildings. In terms of numerical comparisons, the total payments of Case 1, 2, and 3 are 10.4%, 5.7%, and 4.6% higher, respectively, compared to Case 4.

Table 3. Economic comparison of different cases.

Case	Payment to the Consumers	Payment to the Grid	Total Payment
1	0 USD	1703.3 USD	1703.3 USD
2	92.3 USD	1537.4 USD	1629.7 USD
3	0 USD	1613.2 USD	1613.2 USD
4	89.3 USD	1453.1 USD	1542.4 USD

The curves of HVAC power under different operation modes are shown in Figure 7. In Case 2, the HVAC needs to maintain the room temperature at a fixed value, which is 22 °C in this section. Thus, the flexibility of HVACs and the thermal inertia of buildings have not been fully explored. The weak sensitivity of humans to small changes in temperature has not been fully utilized. Case 4 allows the room temperature to fluctuate within an acceptable range for consumers, bringing considerable adjustable margin to HVAC power. It can be seen from Figure 7 that the HVAC power of Case 4 is lower than Case 2 at peak periods of power price and higher than Case 2 at valley periods of power price. This is because the proposed strategy utilizes the thermal inertia of buildings to store heat in advance during periods of low power prices, thereby reducing HVAC power during peak periods of power price and then decreasing power purchase costs. The temperature curves are shown in Figure 8. In Case 2, the room temperature curve is a horizontal line, which means the indoor temperature remains at a stable level, evidencing that the supply air temperature fluctuates with the outdoor temperature. The lower the ambient temperature, the higher the supply air temperature. In Case 4, as mentioned above, smart buildings store heat by increasing indoor temperature to save on power payments, resulting in an additional increase in supplied air temperature on the basis of fluctuations with outdoor temperature.
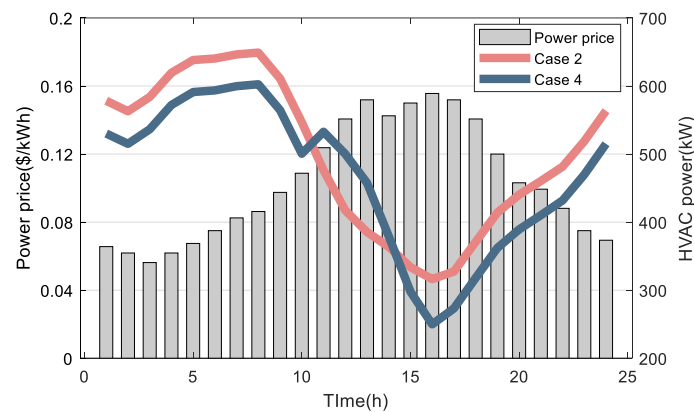
Figure 7. Power consumption of HVACs.
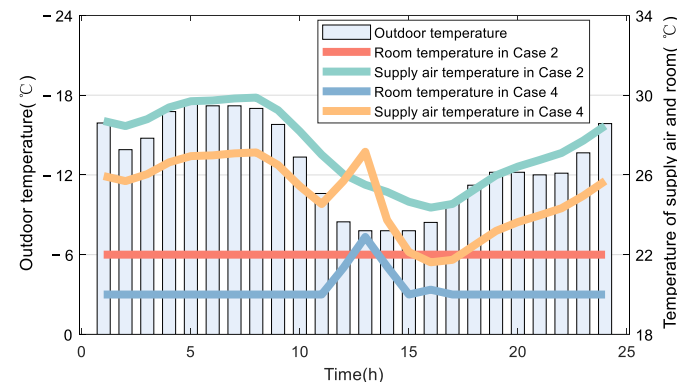
Figure 8. Room temperature and supply air temperature of HVACs.

Ambient temperature is a crucial factor influencing the HVAC system operation that can significantly affect the energy consumption of smart buildings. Figure 9 illustrates the change in HVAC power caused by decreasing different temperatures from the original outdoor temperature (shown in Figure 4). As we can see, the trends of the curves are similar, but lower outdoor temperatures result in higher HVAC power. This is because lower outdoor temperatures cause more heat to be lost from the buildings, requiring higher heating power of HVACs to maintain users' needs.
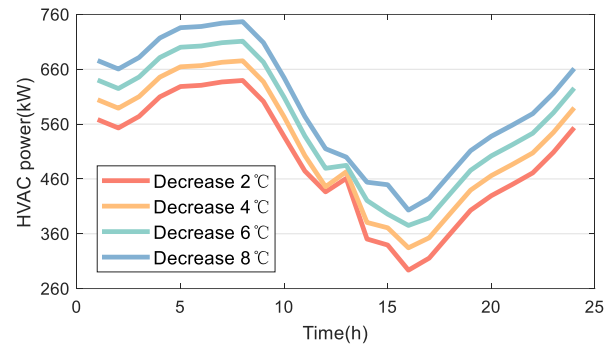
Figure 9. HVAC power with different outdoor temperatures.

Moreover, the differences between fixed and time-variant power prices are compared in Table 4, ensuring the mean values of power prices in these two cases are the same. As we can see, the total payment for the building energy system with time-variant power prices is lower. Since the advantage of smart buildings is they can adjust the strategies according to the fluctuations in power prices, they reduce operating costs. If the power prices are fixed, the flexibility of smart buildings is not fully utilized, leading to a lower payment to the consumers and a higher payment to the grid.

Table 4. Economic comparison between the cases with fixed prices and time-variant prices.

Power Price	Payment to the Consumers	Payment to the Grid	Total Payment
Fixed	33.1 USD	1793.0 USD	1826.1 USD
Time-variant	89.3 USD	1453.1 USD	1542.4 USD

In addition to HVACs, reducing and transferring loads can also flexibly respond to changes in power prices. The effects comparison is shown in Figure 10. As we can see, Case 4 curtails part of the loads and transfers some loads out of the peak periods of power price. Therefore, compared to Case 3, loads in Case 4 are more distributed in periods of low power price rather than periods of high power price, which can further decrease the economic cost of smart buildings.
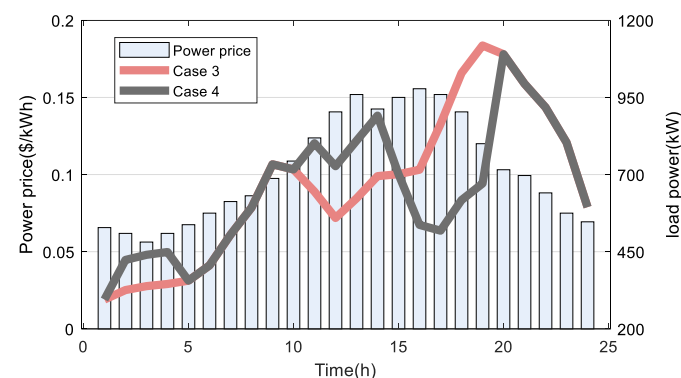
Figure 10. Electrical loads after curtailments and transfers.

The ESS can reduce the impact of PV uncertainty to a certain extent. The ESS power is shown in Figure 11, where positive values mean charging power and negative values mean discharging power. As shown in the figure, ESS experiences three charging behaviors. The first time is to replenish energy to ESS in advance during the low power price periods. The second time occurs when there is excess power caused by high PV output. The last time is to supplement the SOC of ESS to the initial value. The ESS in other time periods operates on discharging mode to support the loads of smart buildings. In Case 4, the total payments with and without ESS are USD 1542.4 and USD 1649.9, respectively, which also confirms the importance of ESS for the economic operation of smart buildings.
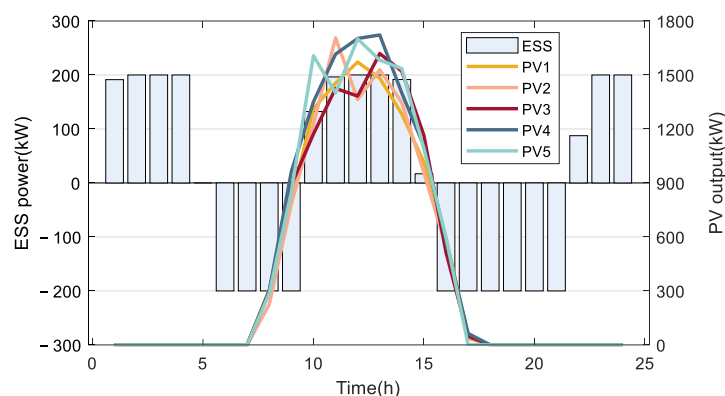
**Figure 11.** Charging and discharging power of the ESS.

For different parameters of the energy storage system, we carried out the corresponding comparative validation, which is shown in Table 5. It can be concluded that the decrease in maximum power of charging and discharging, charging and discharging efficiency, and energy capacity will increase the total payment, which means less economy.

Table 5. Economic comparison among the cases with different parameters of the ESS.

Maximum Power of Charging and Discharging	Charging and Discharging Efficiency	Energy Capacity	Total Payment
200 kW	0.95	2000 kWh	1542.4 USD
160 kW	0.95	2000 kWh	1558.4 USD
200 kW	0.90	2000 kWh	1558.7 USD
200 kW	0.95	1500 kWh	1547.3 USD

The purchased power from the grid is shown in Figure 12. Case 4 requires the least amount of power to be purchased during peak power price periods, while Case 1 requires the most. This is also one of the reasons that Case 4 has the best economy. Moreover, the peak–valley differences of transformer load are shown in Table 6. It can be seen that Cases 3 and 4 have a smaller peak–valley difference than Cases 1 and 2, indicating the time-lag characteristics of the adjustable indoor temperature give a larger margin to HVAC to reduce the peak–valley difference.

To explore the influence of consumers' comfort ranges on the operation of smart buildings, the impact of different range sizes on the economy is compared, and the results are shown in Table 7. As the consumers' comfort range gradually expands, the economic cost of smart buildings gradually decreases. This is because the larger the temperature comfort range, the more it can fully utilize the thermal inertia of the building and the flexible regulation ability of HVACs, thereby improving the operational status of smart buildings.
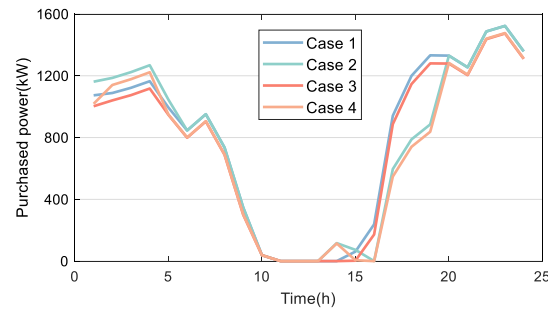
Figure 12. Purchased power from grid in different cases.

Table 6. Comparison of peak–valley differences.

Case	Peak–Valley Difference
1	395.20 kW
2	395.20 kW
3	389.66 kW
4	390.47 kW

Table 7. Comparison of different consumers' comfort ranges.

Consumers' Comfort Range	Total Payment
24–26 °C	1712.6 USD
22–28 °C	1626.8 USD
20–30 °C	1542.4 USD

To verify the scalability and effectiveness of the proposed strategy, a comparative analysis is conducted on smart building aggregation of different scales. The results are shown in Table 8. Among smart building aggregations of different scales, Case 4 still has the best economy, and its advantages become more significant as the scale increases.

Table 8. Comparison of different scales of smart building aggregations.

The Number of Buildings	Case	Total Payment
10	Case 1	2288.2 USD
	Case 2	2232.6 USD
	Case 3	2172.6 USD
	Case 4	2114.2 USD
20	Case 1	5803.3 USD
	Case 2	5647.9 USD
	Case 3	5528.3 USD
	Case 4	5374.7 USD
30	Case 1	9431.7 USD
	Case 2	9198.1 USD
	Case 3	9019.2 USD
	Case 4	8785.6 USD

To verify the superiority of the DRO-based operation model of the building energy system, the comparison between stochastic programming, robust optimization, and DRO is conducted. Figure 13 shows the economy of the building energy system with different sample sizes. From the figure, we can see that the cost of DRO falls between the costs of stochastic programming and robust optimization, which means the adopted method is neither overly conservative like robust optimization, nor overly optimistic like stochastic programming. Table 9 shows the in-sample cost and out-of-sample costs of DRO and stochastic programming. As we can see, the larger the sample size, the lower the in-sample

and expected out-of-sample costs of DRO. For stochastic programming, the larger the sample size, the higher the in-sample cost, but the lower the expected out-of-sample cost.
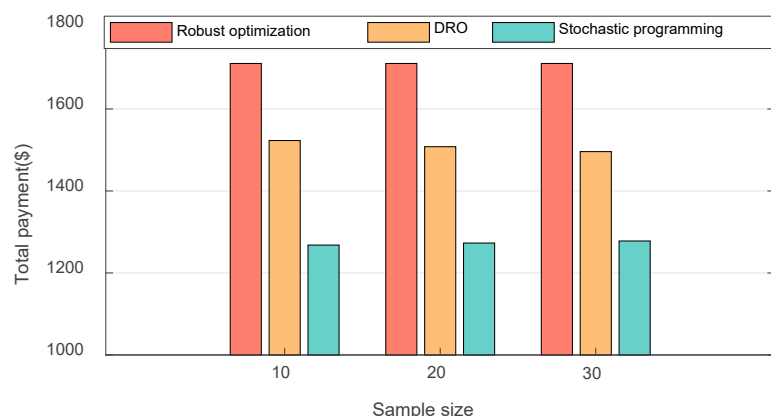
Figure 13. Comparison of different methods.

Table 9. Numerical comparison between DRO and stochastic programming.

Method	DRO		Stochastic Programming	
Sample Size	In-Sample Cost (USD)	Out-of-Sample Mean (USD)	In-Sample Cost (USD)	Out-of-Sample Mean (USD)
10	1523.2	1510.3	1268.3	1275.6
20	1508.5	1492.9	1273.1	1284.2
30	1496.7	1483.6	1278.0	1292.9

5. Conclusions

This paper proposes a data-driven distributionally robust optimization-based DR in heterogeneous building energy systems with rooftop renewables under cold climates. Considering consumers' comfortable temperature range and the uncertainty of PV output, the proposed strategy flexibly schedules curtailable loads, transferrable loads, and HVAC power based on cooperative complementarity and flexible transformation characteristics. The ambiguity set of rooftop PV's probability distribution is constructed by the Wasserstein metric, and then the original DRO model is reformulated into a computational tractable mixed-integer linear programming. Through comparative analysis under different strategies and operating conditions, the following conclusions can be drawn:

(1) By fully utilizing the thermal inertia of buildings, heat can be pre-stored within the indoor space, enabling the flexible adjustment of HVAC power while meeting consumers' temperature comfort requirements. This leads to reduced operating costs for smart buildings. Compared to Case 2, the economic cost in Case 4, which incorporates adjustable indoor temperature, is reduced by 87.3 USD.

(2) Curtailable and transferrable loads play a crucial role in responding to changes in power prices. By reducing load power during periods of high electricity prices, the operational economy of smart buildings can be further improved. Compared to Case 3, the economic cost in Case 4 with curtailable loads and transferrable loads is reduced by 70.8 USD.

(3) The flexibility and economy of smart buildings increase as the acceptable temperature range for consumers expands. When the temperature range expands from 24–26 °C to 20–30 °C, the economic cost decreases by 170.2 USD. Furthermore, the proposed strategy is applicable to smart building aggregations of various scales, and its superiority becomes increasingly significant as the scale expands. When the building scale increases from 10 to 30, the cost difference between Case 1 and Case 4 grows from 174 USD to 646.1 USD.

References

1. Harish, V.; Kumar, A. A Review on Modeling and Simulation of Building Energy Systems. *Renew. Sustain. Energy Rev.* **2016**, *56*, 1272–1292. [CrossRef]
2. Gehbauer, C.; Lee, E.S.; Wang, T. An Evaluation of the Demand Response Potential of Integrated Dynamic Window and HVAC Systems. *Energy Build.* **2023**, *298*, 113481. [CrossRef]
3. IEA. *World Energy Outlook 2023*; International Energy Agency: Paris, France, 2023; pp. 1–355.
4. Jurjevic, R.; Zakula, T. Demand Response in Buildings: A Comprehensive Overview of Current Trends, Approaches, and Strategies. *Buildings* **2023**, *13*, 2663. [CrossRef]
5. Hou, Q.; Zhang, N.; Du, E.; Miao, M.; Peng, F.; Kang, C. Probabilistic Duck Curve in High PV Penetration Power System: Concept, Modeling, and Empirical Analysis in China. *Appl. Energy* **2019**, *242*, 205–215. [CrossRef]
6. Humayun, M.; Safdarian, A.; Degefa, M.Z.; Lehtonen, M. Demand Response for Operational Life Extension and Efficient Capacity Utilization of Power Transformers during Contingencies. *IEEE Trans. Power Syst.* **2014**, *30*, 2160–2169. [CrossRef]
7. Olsen, D.J.; Sarker, M.R.; Ortega-Vazquez, M.A. Optimal Penetration of Home Energy Management Systems in Distribution Networks Considering Transformer Aging. *IEEE Trans. Smart Grid* **2016**, *9*, 3330–3340. [CrossRef]
8. Chen, Y.; Chen, Z.; Yuan, X.; Su, L.; Li, K. Optimal Control Strategies for Demand Response in Buildings Under Penetration of Renewable Energy. *Buildings* **2022**, *12*, 371. [CrossRef]
9. Kharrazi, A.; Sreeram, V.; Mishra, Y. Assessment Techniques of the Impact of Grid-Tied Rooftop Photovoltaic Generation on the Power Quality of Low Voltage Distribution Network—A Review. *Renew. Sustain. Energy Rev.* **2020**, *120*, 109643. [CrossRef]
10. Ghaleb, B.; Asif, M. Assessment of Solar PV Potential in Commercial Buildings. *Renew. Energy* **2022**, *187*, 618–630. [CrossRef]
11. Kapsalis, V.; Maduta, C.; Skandalos, N.; Wang, M.; Bhuvad, S.S.; D'Agostino, D.; Ma, T.; Raj, U.; Parker, D.; Peng, J.; et al. Critical Assessment of Large-Scale Rooftop Photovoltaics Deployment in yhe Global Urban Environment. *Renew. Sustain. Energy Rev.* **2024**, *189*, 114005. [CrossRef]
12. Kiss, V.M.; Hetesi, Z.; Kiss, T. The Effect of Time Resolution on Energy System Simulation in Case of Intermittent Energies. *Renew. Sustain. Energy Rev.* **2024**, *191*, 114099. [CrossRef]
13. Oh, S.; Kong, J.; Yang, Y.; Jung, J.; Lee, C.H. A Multi-Use Framework of Energy Storage Systems Using Reinforcement Learning for Both Price-Based and Incentive-Based Demand Response Programs. *Int. J. Electr. Power* **2023**, *144*, 108519. [CrossRef]
14. Kansal, G.; Tiwari, R. A PEM-Based Augmented IBDR Framework and Its Evaluation in Contemporary Distribution Systems. *Energy* **2024**, *296*, 131102. [CrossRef]
15. Roy, N.B.; Das, D. Stochastic Power Allocation of Distributed Tri-Generation Plants and Energy Storage Units in a Zero Bus Microgrid with Electric Vehicles and Demand Response. *Renew. Sustain. Energy Rev.* **2024**, *191*, 114170. [CrossRef]
16. Deng, R.; Yang, Z.; Chow, M.Y.; Chen, J. A Survey on Demand Response in Smart Grids: Mathematical Models and Approaches. *IEEE Trans. Ind. Inform.* **2015**, *11*, 570–582. [CrossRef]
17. Cruz, C.; Tostado-Véliz, M.; Palomar, E.; Bravo, I. Pattern-Driven Behaviour for Demand-Side Management: An Analysis of Appliance Use. *Energy Build.* **2024**, *308*, 113988. [CrossRef]
18. Strezoski, L.; Stefani, I. Enabling Mass Integration of Electric Vehicles through Distributed Energy Resource Management Systems. *Int. J. Electr. Power* **2024**, *157*, 109798. [CrossRef]
19. Khajavi, H.; Rastgoo, A. Improving the Prediction of Heating Energy Consumed at Residential Buildings Using a Combination of Support Vector Regression and Meta-Heuristic Algorithms. *Energy* **2023**, *272*, 127069. [CrossRef]
20. Lu, N. An Evaluation of the HVAC Load Potential for Providing Load Balancing Service. *IEEE Trans. Smart Grid* **2012**, *3*, 1263–1270. [CrossRef]

21. Lü, X.; Lu, T.; Kibert, C.J.; Viljanen, M. Modeling and Forecasting Energy Consumption for Heterogeneous Buildings Using a Physical–Statistical Approach. *Appl. Energy* **2015**, *144*, 261–275. [CrossRef]

22. Erdinc, O.; Taşcıkaraoğlu, A.; Paterakis, N.G.; Eren, Y.; Catalão, J.P. End-Consumer Comfort Oriented Day-Ahead Planning for Responsive Residential HVAC Demand Aggregation Considering Weather Forecasts. *IEEE Trans. Smart Grid* **2016**, *8*, 362–372. [CrossRef]

23. Lin, J.; Sun, J.; Feng, Y.; Zheng, M.; Yu, Z. Aggregate Demand Response Strategies for Smart Communities with Battery-Charging/Switching Electric Vehicles. *J. Energy Storage* **2023**, *58*, 106413. [CrossRef]

24. Mansouri, S.A.; Paredes, Á.; González, J.M.; Aguado, J.A. A Three-Layer Game Theoretic-Based Strategy for Optimal Scheduling of Microgrids by Leveraging a Dynamic Demand Response Program Designer to Unlock the Potential of Smart Buildings and Electric Vehicle Fleets. *Appl. Energy* **2023**, *347*, 121440. [CrossRef]

25. Li, H.; Wan, Z.; He, H. Real-Time Residential Demand Response. *IEEE Trans. Smart Grid* **2020**, *11*, 4144–4154. [CrossRef]

26. Zhang, Y.; Huang, Z.; Zheng, F.; Zhou, R.; Le, J.; An, X. Cooperative optimization scheduling of the electricity-gas coupled system considering wind power uncertainty via a decomposition-coordination framework. *Energy* **2020**, *194*, 116827. [CrossRef]

27. Li, Y.; Li, K.; Yang, Z.; Yu, Y.; Xu, R.; Yang, M. Stochastic Optimal Scheduling of Demand Response-Enabled Microgrids with Renewable Generations: An Analytical-Heuristic Approach. *J. Clean. Prod.* **2022**, *330*, 129840. [CrossRef]

28. Mansy, H.; Kwon, S. Optimal HVAC Control for Demand Response via Chance-Constrained Two-Stage Stochastic Program. *IEEE Trans. Smart Grid* **2020**, *12*, 2188–2200. [CrossRef]

29. Ding, B.; Li, Z.; Li, Z.; Xue, Y.; Chang, X.; Su, J.; Jin, X.; Sun, H. A CCP-based distributed Cooperative Operation Strategy for Multi-Agent Energy Systems Integrated with Wind, Solar, and Buildings. *Appl. Energy* **2024**, *365*, 123275. [CrossRef]

30. Zhao, C.; Wan, C.; Song, Y. An Adaptive Bilevel Programming Model for Nonparametric Prediction Intervals of Wind Power Generation. *IEEE Trans. Power Syst.* **2019**, *35*, 424–439. [CrossRef]

31. Yang, X.; Chen, Z.; Huang, X.; Li, R.; Xu, S.; Yang, C. Robust Capacity Optimization Methods for Integrated Energy Systems Considering Demand Response and Thermal Comfort. *Energy* **2021**, *221*, 119727. [CrossRef]

32. Li, Z.; Wu, L.; Xu, Y.; Zheng, X. Stochastic-Weighted Robust Optimization based Bilayer Operation of a Multi-Energy Building Microgrid Considering Practical Thermal Loads and Battery Degradation. *IEEE Trans. Sustain. Energy* **2022**, *13*, 668–682. [CrossRef]

33. Mohajerin Esfahani, P.; Kuhn, D. Data-Driven Distributionally Robust Optimization Using the Wasserstein Metric: Performance Guarantees and Tractable Reformulations. *Math. Program.* **2018**, *171*, 115–166. [CrossRef]

34. Huang, H.; Li, Z.; Gooi, B.; Qiu, H.; Zhang, X.; Lv, C.; Liang, R.; Gong, D. Distributionally Robust Energy-Transportation Co-ordination in Coal Mine Integrated Energy Systems. *Appl. Energy* **2023**, *333*, 120577. [CrossRef]

35. Huang, Z.; Wang, F.; Lu, Y.; Chen, X.; Wu, Q. Optimization model for home energy management system of rural dwellings. *Energy* **2023**, *283*, 129039. [CrossRef]

36. Li, J.; Khodayar, M.E.; Wang, J.; Zhou, B. Data-Driven Distributionally Robust Co-Optimization of P2P Energy Trading and Network Operation for Interconnected Microgrids. *IEEE Trans. Smart Grid* **2021**, *12*, 5172–5184. [CrossRef]

37. Hanasusanto, G.A.; Kuhn, D. Conic Programming Reformulations of Two-Stage Distributionally Robust Linear Programs over Wasserstein Balls. *Oper. Res.* **2018**, *66*, 849–869. [CrossRef]